# Triple helix versus skyrmion lattice in two-dimensional noncentrosymmetric magnets

V. E. Timofeev,[1,2,*] A. O. Sorokin,[1] and D. N. Aristov[1,3]
[1]*NRC Kurchatov Institute, Petersburg Nuclear Physics Institute, Gatchina 188300, Russia*
[2]*St. Petersburg Electrotechnical University LETI, 197376 St. Petersburg, Russia*
[3]*St. Petersburg State University, 7/9 Universitetskaya nab., 199034 St. Petersburg, Russia*

(Received 2 October 2020; revised 29 January 2021; accepted 18 February 2021; published 1 March 2021)

It is commonly assumed that a lattice of skyrmions, emerging in two-dimensional noncentrosymmetric magnets in external magnetic fields, can be represented as a sum of three magnetic helices. To test this assumption, we compare two approaches to a description of a regular skyrmion structure. We construct (i) a lattice of Belavin-Polyakov-like skyrmions within the stereographic projection method and (ii) a deformed triple helix defined with the use of elliptic functions. The estimates for the energy density and magnetic profiles show that these two ansatzes are nearly identical at zero temperature for intermediate magnetic fields. However, at higher magnetic fields, near the transition to a topologically trivial uniform phase, the stereographic projection method is preferable, particularly for the description of a disordered skyrmion liquid phase. We suggest exploring the intensities of secondary Bragg peaks to obtain additional information about the magnetic profile of individual skyrmions. We estimate these intensities to be several percent of the main Bragg peak at high magnetic fields.

DOI: 10.1103/PhysRevB.103.094402

## I. INTRODUCTION

Topologically protected states of matter attract the attention of researchers from various fields of science. One of the well-known examples of topologically protected objects is skyrmions. Despite the fact that the first appearance of skyrmions is associated with particle physics [1], the study of magnetic skyrmions has become a rapidly developing field of condensed-matter physics over the last decade [2,3]. The most discussed magnetic skyrmions are nanoscale vortex-like configurations. The relatively small size of skyrmions makes them promising objects for developing new types of data storage devices [4,5]. According to the Hobart-Derrick theorem [6], topological arguments alone are not enough to stabilize skyrmions, while additional conditions are needed to fix a skyrmion size. Usually, a single skyrmion or an unordered set of skyrmions can be stabilized in a finite sample: a disk [7] or a track (nanoribbon) [8]. In this case, the stability of skyrmions is provided by the dipole-dipole interaction and surface effects. For an infinite system, the stabilization of skyrmions is achieved in noncentrosymmetric magnets, where the combination of the Dzyaloshinskii-Moriya interaction (DMI) [9] and an applied magnetic field lead to the existence of long-period modulated magnetic phases, so single skyrmions appear as elements of a so-called skyrmion crystal (SkX) [10]. Probably the best studied class of noncentrosymmetric magnets is $B20$ compounds, including MnSi, etc. [11].

Experimental investigations of such compounds show that the skyrmion phase in the bulk (also called A phase) exists at finite temperatures, slightly below the critical one, $T_C$. Thermal fluctuations are expected to play a crucial role in the stability of the A phase [11]. This phase is observed at moderate magnetic fields, with its phase boundary far away from the critical (saturation) field. The intensity maps of neutron scattering experiments show a hexagonal pattern of Bragg peaks in the A-phase region. It allows us to interpret the A-phase spin configuration in two ways: either as a hexagonal skyrmion superlattice or as a sum of three simple helices with wave vectors directed at an angle of 120° relative to each other [11]. These two descriptions are not equivalent and may be distinguished in experiments, but the corresponding difference may be hidden by the experimental specifics and thermal modulation of the local magnetization [12]. The latter reason makes thin-film investigations more preferable, where the A phase is more stable and exists [13] at $T \approx 0$.

It is known that the correspondence between long-period modulated phases (like a helix) and phases with a finite soliton density may be exact. One such example happens in one spatial dimension, where skyrmions are kinks in the sine-Gordon model [14,15]. A one-dimensional magnet with uniaxial anisotropy, DMI, and an external field is described by the sine-Gordon model with the Lifshitz invariants. This model has been exactly solved by Dzyaloshinskii as a modified helical configuration in terms of Jacobi elliptic functions [16]. As an alternative (dual) description of this solution, one can consider a lattice of kinks [17–19].

The two-dimensional case is more difficult for modeling. Due to nonlinearity, the triple helix anzatz as a sum of three helices is not an exact solution for the ground state at $T = 0$. Moreover, one can propose several ways to construct a triple helix configuration. The simplest way, usually found in literature (see, e.g., Refs. [11,20]) is a sum of ordinary (nonmodified) helices [21].

Recently, we showed [22] that the stereographic projection method provides a very good estimate of the ground-state energy and the shape of the individual skyrmions remains nearly

*timofeeviktor@gmail.com

 

invariant under pressure from its neighbors. The advantage of the latter method is its flexibility that concerns the positions and sizes of individual skyrmions. One can particularly employ this description for the skyrmion liquid state reported previously in Refs. [23,24] at some magnetic fields.

In this paper, we examine different descriptions of skyrmion lattice states in two dimensions at zero temperature. In Sec. II, we describe the stereographic approach for the SkX construction. In Sec. III, we remind the reader of a general form of the magnetic helix for systems with DMI and magnetic field in terms of the additional elliptic parameter [25]. With this generalization, we construct the triple helix ansatz in Sec. IV at $T = 0$ with normalization conditions for the local magnetization. In Sec. V, we compare the modeling by SkX and triple helix with respect to density of classical energy, the period of the spatial modulation, and intensities of higher-order Bragg peaks. Our final remarks are presented in Sec. VI.

## II. SKYRMION CRYSTAL

We consider the two-dimensional system characterized by magnetization $\mathbf{S}(\mathbf{r})$. At zero temperature, the magnetization is saturated and can be normalized, $\mathbf{S}^2 = 1$. The classical energy density in the standard model of chiral magnets is

$$\mathcal{E} = \tfrac{1}{2}C\partial_\mu S^i \partial_\mu S^i - D\epsilon_{\mu ij} S^i \partial_\mu S^j + B(1 - S^3), \qquad (1)$$

where $\mu = 1, 2$ and $i = 1, 2, 3$. The first term corresponds to the FM exchange, the second one is DMI, and the last one is the Zeeman energy related to an external magnetic field perpendicular to the plane. The main spatial scale in this model is defined by $L = C/D$ and the energy scale is $D^2/C$. After appropriate rescaling, Eq. (1) reads

$$\mathcal{E} = \tfrac{1}{2}\partial_\mu S^i \partial_\mu S^i - \epsilon_{\mu ij} S^i \partial_\mu S^j + b(1 - S^3), \qquad (2)$$

with the dimensionless magnetic field $b = CB/D^2$.

A single skyrmion is an axially symmetric solution with a unit topological charge. Multiskyrmion configurations can be described in the stereographic projection approach [22], which is a convenient way to take into account the interaction between skyrmions and construct fully periodic configuration of SkXs. In this section, we sketch the main idea of such consideration.

For the normalized solution, one can write

$$S^1 + iS^2 = \frac{2f(z,\bar{z})}{1 + f(z,\bar{z})\bar{f}(z,\bar{z})}, \quad S^3 = \frac{1 - f(z,\bar{z})\bar{f}(z,\bar{z})}{1 + f(z,\bar{z})\bar{f}(z,\bar{z})}, \qquad (3)$$

where $f(z,\bar{z})$ is a complex-valued function of $z = x + iy$ and $\bar{z} = x - iy$. It was noticed early on [26] that every holomorphic or antiholomorphic function is a solution of the model without both DMI and an external magnetic field. One can check in the latter case that one skyrmion corresponds to $f = z_0/\bar{z}$ and that $N$-skyrmion solutions are given by $f = \sum_{j=1}^{N} z_0^j/(\bar{z} - \bar{z}_j)$; here $z_0^j$ define radii and orientation of individual skyrmions.

When we discuss the single skyrmion solution, the addition of DMI and external field may lead to continuous transformation of the Belavin–Polyakov (BP) solution, without changing the character of singularities. Our ansatz for the single skyrmion solution is given by

$$f(z,\bar{z}) = \frac{e^{i\alpha}\kappa(z\bar{z})}{\bar{z}}, \qquad (4)$$

where phase $\alpha$ is eventually determined by the sign of the DMI, and a singularity-free function $\kappa(z\bar{z})$ depends smoothly on the distance from the skyrmion's center.

The equation for $\kappa$ is quite nonlinear and can be solved only numerically. Since $\kappa$ has the dimension of length, we choose to consider a dimensionless function $\tilde{\kappa}(y) = (\kappa(0))^{-1}\kappa(y\,\kappa(0)^2)$ with the property $\tilde{\kappa}(0) = 1$. One could then solve the equation for $\tilde{\kappa}(y)$ for different boundary conditions. Our primary interest is to find $\tilde{\kappa}(y)$ on a disk of finite radius which mimics the case of SkXs where one skyrmion is surrounded by its neighbors. The pressure exerted by this type of environment is modeled by changing the size of a disk. We found that the function $\tilde{\kappa}(y)$ is nearly invariant against changes of the disk radius, in contrast to the value of the dimensionless residue, $\kappa(0)/L$. One hence can model multiskyrmion configurations by the sum

$$f(z,\bar{z}) = \sum_j F\left((\bar{z} - \bar{z}_j)/z_0^{(j)}\right), \qquad (5)$$

where

$$F\left(\frac{\bar{z}}{z_0}\right) \equiv \frac{z_0}{\bar{z}}\tilde{\kappa}_\infty\left(\left|\frac{\bar{z}}{z_0}\right|^2\right), \qquad (6)$$

where $\kappa_\infty$ is the solution on the disk of infinite radius, and $|z_0|$ in this formula is the skyrmion's size. We remind the reader that the formula Eq. (5) with arbitrary $z_j$, $z_0^{(j)}$ provided an exact (metastable) solution to (1) at $D = B = 0$. In that case, skyrmions did not interact and the energy was given by $\mathcal{E} = \sum_j \mathcal{E}[f_j]$ with the energy of individual skyrmions (chemical potential) $\mathcal{E}[f_j] \equiv 4\pi C$. Both DMI and the magnetic field bring characteristic scales into the model that results in the interaction between skyrmions, which is the main difference between the model Eq. (1) and BP model.

We perform the exact numerical calculation of the energy density for SkX modeled by Eq. (5) with the use of formulas Eqs. (1)–(6), for the most interesting case of densely packed SkXs by putting $\bar{z}_j$ onto triangular lattice. The energy density calculated within the (hexagonal) unit cell of such a SkX has two parameters: the unit cell parameter or period of the lattice, $a$, and the radius of the skyrmion, $|z_0|$; one should minimize the density, $\rho = 2/\sqrt{3}E_{\text{cell}}(z_0, a)/a^2$ over $a$ and $|z_0|$. We present the results of this minimization below in Fig. 2 and compare it with other model configurations.

Earlier we showed [22] that the energy of configuration Eq. (5) can be regarded as the sum of (i) the energies of individual skyrmions, $\mathcal{E}[f_j]$, (ii) the pairwise (repulsive) interactions between them, $U_2(z_0, a) = \mathcal{E}[f_1 + f_2] - \mathcal{E}[f_1] - \mathcal{E}[f_2]$, and (iii) the remaining part, $U_3$, which does not fit to these two categories. Because of strong nonlinear effects of the model, $U_3$ turns out to be sizable (and attractive) and largely corresponds to the triple interaction between the nearest skyrmions. Interestingly, as first noticed in Ref. [22], the exact calculation of the optimal energy per unit cell corresponds with the overall accuracy $10^{-3}$ to the approximate

expression

$$E_{\text{cell}}(z_0, a) = \mathcal{E}[f_1] + 3U_2(z_0, a) + U_3(z_0, a), \quad (7)$$

which takes into account only pairwise and triple interactions between nearest neighbors on the triangular lattice. This surprisingly good approximation means a possibility to discard the contribution from the next-to-nearest neighbors (NNNs). It cannot be fully explained in terms of relative smallness of the pairwise NNN interaction, but rather as a combined effect with the triple NNN interaction of opposite sign. This idea is supported by the observation that the calculated energy in the hexagonal cell around a skyrmion with its six neighbors is nearly identical to the energy, calculated for this configuration with six added NNN skyrmions.

## III. SINGLE HELIX

The well-known expression [21] for a single helix configuration in magnets with DMI is given by

$$\mathbf{S} = \hat{c}\cos\alpha + [\hat{b}\cos(\mathbf{kR} + \beta) + \hat{a}\sin(\mathbf{kR} + \beta)]\sin\alpha\,, \quad (8)$$

where $\hat{a}, \hat{b}, \hat{c}$ are unit vectors with $\hat{a} = \hat{b} \times \hat{c}$, $\mathbf{k}$ is the helix propagation vector and $\alpha$ is the cone angle. Equation (8) is the starting point for analysis of all helical states: conical, cycloidal, etc. The main question of such an analysis is the choice of $\hat{\mathbf{k}}, \hat{a}, \hat{b}, \hat{c}$, the values of $k$ and $\theta$. All these parameters are determined by particular form of the Hamiltonian, crystal symmetries, etc.

We are interested in the 2D spatial case, so $\mathbf{k}$ lies in a plane. Parametrizing the basis as $\hat{a} = (-\sin\varphi, \cos\varphi, 0)$, $\hat{b} = (-\cos\theta\cos\varphi, \cos\theta\sin\varphi, \sin\theta)$ and $\hat{c} = (\cos\varphi\sin\theta, \sin\varphi\sin\theta, \cos\theta)$, one can show for arbitrary DMI that in the 2D case the vector $\hat{c}$ lies in a plane, $\theta = \pi/2$, and the cone angle collapses, $\alpha = \pi/2$. It means that the spin configuration becomes

$$\mathbf{S}_\varphi = \begin{pmatrix} \sin\varphi\sin(\mathbf{k}_\varphi\mathbf{R}) \\ -\cos\varphi\sin(\mathbf{k}_\varphi\mathbf{R}) \\ \cos(\mathbf{k}_\varphi\mathbf{R}) \end{pmatrix}. \quad (9)$$

The angle $\varphi$ defines the plane of magnetization rotation and in turn determines the direction of $\mathbf{k}_\varphi$ for a particular form of DMI. In this paper, we use the relation

$$\mathbf{k}_\varphi = k(\cos\varphi, \sin\varphi, 0)\,,$$

appropriate for our 2D model Eq. (1). This case is realized in the case of cubic symmetry of crystal (B20 compounds, for example), where Dzyaloshinskii vector is parallel to bonds. Different types of crystal symmetries could lead to different forms of DMIs, and the relation between $\mathbf{k}_\varphi$ and $\varphi$ could be different.

Actually, in the presence of an external magnetic field perpendicular to the plane, Eq. (8) is not an exact solution of the model [16]. The well-known fact is that in uniaxial magnets with DMI, the simple helix also transforms to the chiral soliton lattice (CSL) [25]. If spins are modulated in the $\hat{x}$ direction and lie in the perpendicular plane, $\mathbf{S} = (0, -\sin\phi(x), \cos\phi(x))$, then the energy Eq. (2) takes the form

$$\mathcal{E} = \tfrac{1}{2}(\partial_x\phi(x))^2 - \partial_x\phi(x) + b(1 - \cos\phi(x))\,, \quad (10)$$

with the resulting Euler-Lagrange equation:

$$\partial_x^2\phi(x) = b\sin\phi(x). \quad (11)$$

This is the sine-Gordon equation having the quasiperiodic solution

$$\phi_0(x) = 2\,\text{am}\left(\sqrt{\frac{b}{m}}x + \beta\middle|m\right) + \pi\,, \quad (12)$$

with the elliptic parameter $m$. The minimization of the energy Eq. (10) links this parameter to the field

$$\frac{E(m)}{\sqrt{m}} = \frac{\pi}{4\sqrt{b}},$$

whereas the energy density at the minimum, $\rho$, and the pitch $k$ are given by expressions [18]

$$\rho = -2b\,\frac{1-m}{m}\,, \quad k = \frac{\pi}{K(m)}\sqrt{\frac{b}{m}}\,. \quad (13)$$

Here $K(m)$ $[E(m)]$ is a complete elliptic integral of the first (second) kind.

Below we expect that the 1D solution Eq. (12) may be convenient for parametrization of the trial function, although the conditions Eqs. (13) do not hold. In this case, we can still use Eq. (12) as a general model form of deformed helix with one control parameter, $m$:

$$\tilde{\mathbf{S}}_\varphi = \begin{pmatrix} -\sin\varphi\ \sin\ 2\,\text{am}\left(\frac{K(m)}{\pi}(\mathbf{k}_\varphi\mathbf{R} + \beta)|m\right) \\ \cos\varphi\ \sin\ 2\,\text{am}\left(\frac{K(m)}{\pi}(\mathbf{k}_\varphi\mathbf{R} + \beta)|m\right) \\ -\cos\ 2\,\text{am}\left(\frac{K(m)}{\pi}(\mathbf{k}_\varphi\mathbf{R} + \beta)|m\right) \end{pmatrix}. \quad (14)$$

This expression is the extension of Eq. (9) with the same spatial period, and additional degree of ellipticity. It coincides with Eq. (9) at $m = 0$, $\beta = \pi$.

## IV. TRIPLE HELIX

In the literature, one can find a statement that a SkX state can be modeled by the sum of three helices with zero sum of helix propagation vectors. In particular, it was argued [11] that thermal fluctuations stabilize the superposition of three helices at high temperatures in the three-dimensional case. Moreover, it has been shown in Ref. [12] that second Bragg peaks in neutron scattering can be mostly attributed to the result of double scattering, and they have insignificant intensities in comparison with the first Bragg peaks.

The simple sum of three helices Eq. (9),

$$\mathbf{S}_{3q} = \mathbf{S}_{\varphi=0} + \mathbf{S}_{\varphi=2\pi/3} + \mathbf{S}_{\varphi=4\pi/3} + S_0\hat{e}_z, \quad (15)$$

has a different magnitude from point to point, i.e., $|\mathbf{S}_{3q}(\mathbf{R})| \neq$ const. For the A phase of 3D compounds, the possibility of this variation can be explained by a closeness to the critical point where the magnitude of magnetization could vary significantly. But in the planar case of our interest at $T = 0$, one should expect the constraint $|\mathbf{S}| = 1$. Below we consider two ways to obtain the normalized triple helix configuration.

### A. Triple helix in the stereographic projection method

As discussed above, the stereographic projection automatically provides the low-temperature normalization constraint

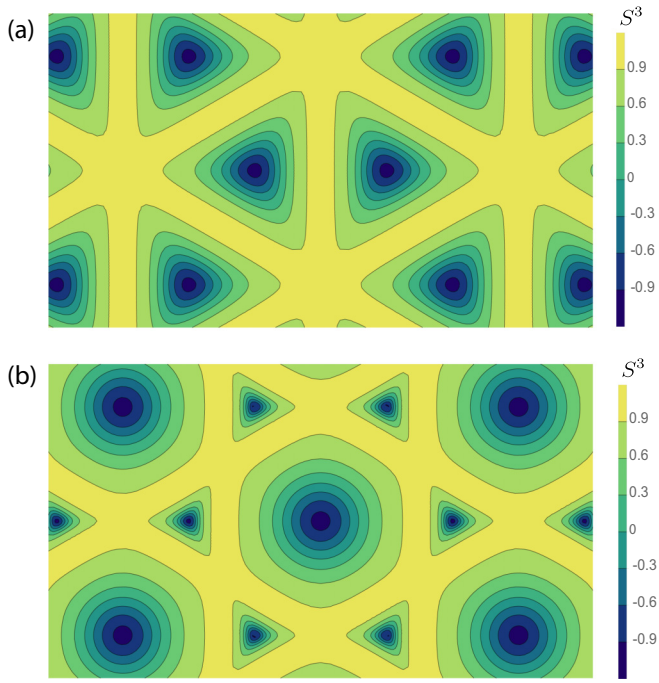


FIG. 1. Schematic pictures of two different types of triple helix structures modeled in stereographic approach: (a) honeycomb lattice appearing for $\beta = \pi$ and (b) kagomé lattice for $\beta = 0$.

$|\mathbf{S}| = 1$, which is convenient for a discussion of multi-skyrmion configurations. It is tempting to also use the method for construction of a multiple-helix configuration.

One can easily verify that the single helix Eq. (14) is represented by the function

$$f_\varphi = ie^{i\varphi} \cot\ \mathrm{am}\left(\frac{K(m)}{\pi}(\mathbf{k}_\varphi \mathbf{R} + \beta)|m\right). \tag{16}$$

This function has a striped structure of zeros and pole lines. The sum of three helices of the form Eq. (16) with different $\mathbf{k}_\varphi$, obeying the relation $\mathbf{k}_{\varphi_1} + \mathbf{k}_{\varphi_2} + \mathbf{k}_{\varphi_3} = 0$, might appear to be a good choice for a description of two-dimensional hexagonal lattices of skyrmions. However, comparing with the previous formula Eq. (5), which has simple poles at the centers of the skyrmions, we choose a different representation in the form

$$f_{3q} = \left(\frac{1}{f_{\varphi=0}} + \frac{1}{f_{\varphi=2\pi/3}} + \frac{1}{f_{\varphi=4\pi/3}}\right)^{-1}. \tag{17}$$

Parameter $m$ now defines the shape of skyrmions and $k$ determines the cell parameter of skyrmion lattice.

In contrast to the combination of two functions, e.g., $f_{2q} = ((f_{\varphi=0})^{-1} + (f_{\varphi=2\pi/3})^{-1})^{-1}$, where an arbitrary value of $\beta$ could be effectively put to zero by an appropriate shift of the origin, the addition of the third helix in Eq. (17) makes the choice of $\beta$ not harmless. As can be seen in Fig. 1, two different configurations of lines of zeros appear, depending on $\beta = \pi$ or $\beta = 0$, corresponding to different topological charge $Q$ per (rhombic) unit cell: for the honeycomb case with $Q = 2$, and for the kagomé case with $Q = 3$.

Our calculation shows that such a construction of the triple helix leads to the higher energy density as one can see from

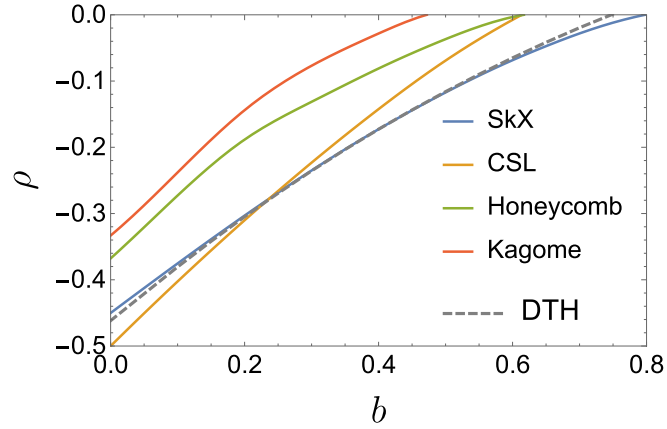


FIG. 2. Density energy for the Hamiltonian Eq. (2) and different spin configurations.

Fig. 2, as compared both to the SkX ansatz from Sec. II and to the variant of triple helix considered in the next subsection. One can argue that the honeycomb lattice configuration in Fig. 1(a) is not tightly packed, which enhances the inter-skyrmion interaction contribution. Such an argument does not hold for the kagomé configuration in Fig. 1(b), where centers of skyrmions form a triangular lattice, similarly to our above ansatz Eq. (5). Our calculation shows that the energy minimization leads to very close estimates in density of topological charge and of Zeeman energy contribution both for Eqs. (17) and (5), whereas the sum of exchange and DMI energy terms is significantly higher in the case of Eq. (17). The latter observation may be associated primarily with the inappropriate size of individual skyrmions in the kagomé configuration, since two out of three skyrmions in the unit cell appear too small for any elliptic index $m$.

### B. Normalized sum of three deformed helices

As discussed in Sec. III, a magnetic field deforms a helix configuration into the more optimal configuration, called a deformed helix or chiral soliton lattice, Eq. (14). It seems then only natural to use a more general combination of three such deformed helices Eq. (14), instead of the simple expression Eq. (15). To be able to compare the energies of different configurations, we should normalize the resulting magnetization:

$$\tilde{\mathbf{S}}_{3q} = \frac{S_0\hat{e}_3 + \tilde{\mathbf{S}}_{\varphi=0} + \tilde{\mathbf{S}}_{\varphi=2\pi/3} + \tilde{\mathbf{S}}_{\varphi=4\pi/3}}{|S_0\hat{e}_3 + \tilde{\mathbf{S}}_{\varphi=0} + \tilde{\mathbf{S}}_{\varphi=2\pi/3} + \tilde{\mathbf{S}}_{\varphi=4\pi/3}|}. \tag{18}$$

We call this expression (taken at $\beta = 0$) the deformed triple helix (DTH) below.

The expression Eq. (18) has three variational parameters for energy minimization: a pitch of helices, $k$, the elliptical parameter, $m$, and the additional magnetization perpendicular to the plane $S_0$. In terms of the resulting SkX structure, the pitch $k$ defines the cell parameter of SkX, while both $m$ and $S_0$ determine the radius and shape of individual skyrmions. Some analysis shows that $S_0$ takes positive values and it is the major parameter defining (and reducing) the size of skyrmions. The role of $m$ is only to adjust the shape of the configuration Eq. (18); in contrast to single helix Eq. (13) with $m \simeq 1$, the

energy minimization by DTH ansatz Eq. (18) yields negative values of $m$ in the whole range of $b$. This might be the reason that the energy difference, $\delta\rho$, between configuration Eq. (18) with $m = 0$ and the one with the optimal value of $m < 0$ is not significant; it is $\delta\rho \approx 0.005$ at smaller $b \simeq 0.3$ while $\delta\rho$ tends to zero near $b \simeq 0.75$.

The energy density found for such an optimal configuration from Eq. (2) is plotted as a function of magnetic field in Fig. 2. In this figure, we also show the energy found for the SkX ansatz Eq. (5) and for the single deformed helix Eq. (14) with optimal parameters. It is seen that at a low external magnetic field $b_{cr1} \lesssim 0.25$, the CSL configuration Eq. (14) is energetically favorable and SkX is advantageous in the intermediate region $b \in (0.25, 0.8)$. In its turn, SkX is destroyed by a magnetic field at $b_{cr2} \approx 0.8$, when the uniform configuration delivers the energy minimum. This calculation is in a good agreement with previous works [10,27]. Two above variants of triple helix in stereographic projection (honeycomb and kagomé) are shown to be higher in energy.

## V. COMPARISON OF THE MODELS

We observe in Fig. 2 that the difference in two descriptions, in terms of SkXs and DTHs, becomes essential in the region of relatively strong magnetic fields. More details can be found in the analysis of the optimal modulation vector for SkXs and DTHs, corresponding to inverse unit cell parameter of SkX, $(4\pi/a\sqrt{3})$, and the pitch, $k$, respectively. The results are presented in Fig. 2; it is seen that the DTH solution becomes increasingly different from SkX in the region of high magnetic fields, $b \in (0.6, 0.8)$. In this region, the SkXs with increasing unit cell parameter is eventually described as a rarified gas of weakly interacting skyrmions, and a dissolution or melting of SkXs happens at the critical field $b = b_{c2}$. At the same time, the DTH model predicts nearly the same value of helical pitch up to $b \simeq 0.73$ when the uniform ferromagnetic (FM) state becomes lower in energy. Considering the density of topological charge $p = k^2\sqrt{3}/8\pi^2$ as an order parameter in the skyrmion phase, one can say that the transition to the FM state in the DTH model corresponds to $p$ abruptly changing to zero. It is instructive to compare this conclusion with SkX ansatz Eq. (5), where the energy of two skyrmions placed at the distance $R$ from each other behaves [22] as $E_2 \simeq 2x + A\exp(-R/\ell)$, with $x \sim b - b_{c2}$, correlation length in the FM state $\ell = b^{-1/2}$ and $A \sim 1$. Minimization of the energy density, $\sim[x + 3A\exp(-R/\ell)]/R^2$ with respect to $R$ leads to $\rho$ depicted in Fig. 2. It also leads to the dependence of topological charge $p \sim (\ell \ln(A/|x|))^{-2}$ and the pitch $k \sim (\ell \ln(A/|x|))^{-1}$ in the vicinity of $b = b_{c2}$. We show the fit by the latter dependence in Fig. 3 by the red dashed line. The dependence of $p$ on $b$ near $b_{c2}$ looks qualitatively the same and we do not show it here.

Note that Fig. 2 indicates the transitions from SkX phase to helical and FM states at $b_{c1} = 0.25$ and $b_{c2} = 0.8$, respectively. According to the recent findings in Ref. [24], additional transitions from skyrmion-solid to skyrmion-hexatic and later to skyrmion-liquid phases happen at intermediate fields in thin films of $Cu_2OSeO_3$ compound. If we associate the upper critical field found in Ref. [24] at low temperatures with $b_{c2}$, then we obtain the values for the additional transitions

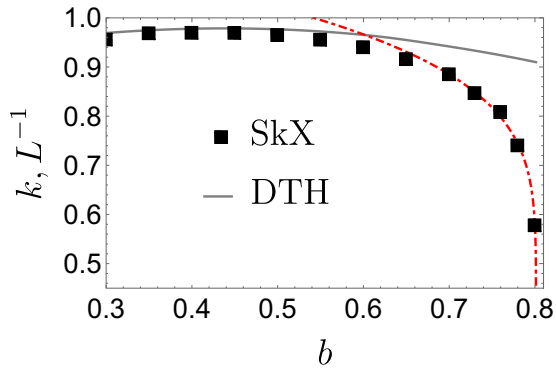


FIG. 3. Optimal value of modulation vector for triple helix and SkX for different values of $b$. The red dashed line is the fit of SkX values of $k$ as described in text.

to be $b = 0.54$ and $b = 0.64$, respectively. Comparing these numbers with our Fig. 3, we see that deviations between our DTH and SkX description happen at higher fields, which correspond to the skyrmion-liquid phase in terms of Ref. [24]. We saw that SkX modeling Eq. (5) provided a better description at higher fields in terms of the energy. We point out an additional advantage of this description in the anticipated skyrmion-liquid phase, because the SkX modeling with Eq. (5) does not require a long-range ordering in positions of skyrmions, in contrast to DTH and other regular helical structures.

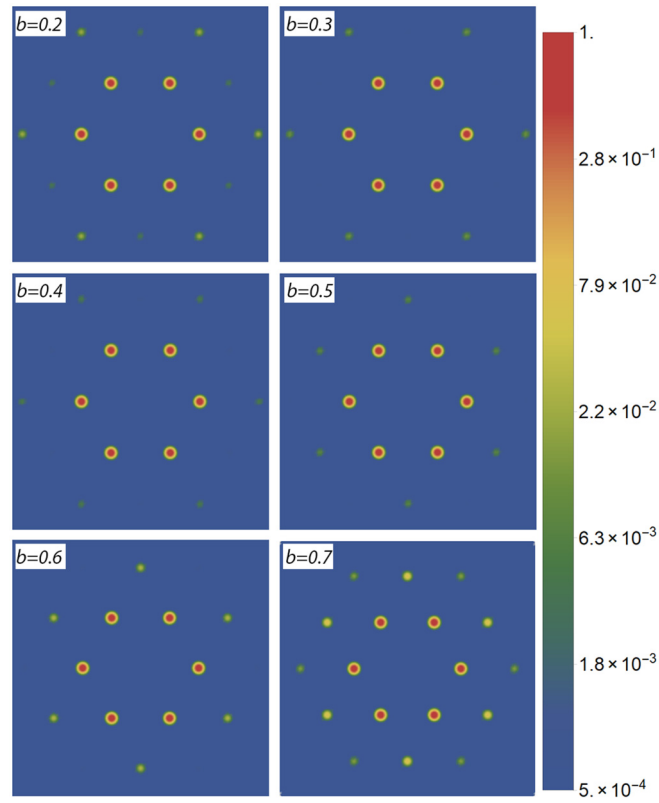


FIG. 4. Maps of predicted intensities for neutron scattering elastic cross section for different magnetic fields, $b$. Delta functions in (20) are approximated by Gaussians. All maps are scaled to the intensity of the first Bragg peaks.

### A. Elastic cross section

The simple formula with a linear combination of three helices Eq. (15) contains only six spatial Fourier harmonics, i.e., only six peaks in the reciprocal space at $\mathbf{k}_\varphi$ with $3\varphi/\pi = 0, \ldots, 5$. This is what is observed experimentally in the high-temperature A phase in bulk materials [11,12]. But, as we discussed above, at low temperature for thin films we should think about normalization of magnetization, and elliptical deformations Eq. (18) should also contain higher harmonics, $\mathbf{k}_{\varphi 1} + \mathbf{k}_{\varphi 2}$.

The cross section of the elastic unpolarized neutron scattering on a magnetic structure is given by [28]

$$\frac{d\sigma}{d\Omega} \propto \sum_{ij} (\delta^{ij} - \hat{q}^i \hat{q}^j) \langle S^i_{\mathbf{q}} \rangle \langle S^j_{-\mathbf{q}} \rangle, \tag{19}$$

with $\langle S^j_{\mathbf{q}} \rangle = \int d\mathbf{r}\, e^{i\mathbf{r}\mathbf{q}} \langle S^j(\mathbf{r}) \rangle$. For periodic structures, such as SkXs and DTH one can represent the cross-section as a sum over reciprocal lattice vectors:

$$\frac{d\sigma}{d\Omega} \propto C_0 + \sum_{m,n} C_{mn} \delta(\mathbf{q} - m\mathbf{b}_1 - n\mathbf{b}_2), \tag{20}$$

here $\mathbf{b}_1 = \mathbf{k}_{\varphi=0}$, $\mathbf{b}_2 = \mathbf{k}_{\varphi=\pi/3}$ and

$$C_{mn} = \sum_{ij} \left( \delta^{ij} - \frac{(mb_1^i + nb_2^i)(mb_1^j + nb_2^j)}{|m\mathbf{b}_1 + n\mathbf{b}_2|^2} \right) \times \langle S^i_{m\mathbf{b}_1 + n\mathbf{b}_2} \rangle \langle S^j_{-m\mathbf{b}_1 - n\mathbf{b}_2} \rangle. \tag{21}$$

We show the maps of predicted intensities in SkX model for different magnetic fields in Fig. 4.

We are interested in relative values of intensities of higher-order Bragg peaks, $C_{mn}/C_{10}$. In our models we find that the magnitude $C_{mn}$ rapidly decreases with $m, n$ so that only $C_{11}/C_{10}$ and $C_{20}/C_{10}$ are of order of few percents, while the other coefficients are even smaller in the whole range of magnetic field. The results of the calculation for different models of our spin texture are shown in Fig. 5. It can be seen in this plot that for magnetic fields in the range $0.3 < b < 0.6$, where SkX and DTH ansatzes yield practically the same energy density, both these models give similar results for $C_{ij}/C_{10}$. This indicates that the spin configuration described by these two approaches is nearly identical.

The situation changes in the region of higher magnetic field $0.65 \lesssim b \lesssim 0.8$, when DTH ansatz fails to reproduce the expected increase in distance between skyrmions. We note that for well-separated skyrmions of a certain shape within the SkX description Eq. (5), the magnitude of the higher peaks $C_{11}$, $C_{20}$ is defined roughly by the Fourier image of an individual skyrmion, $\langle S^i_{\mathbf{q}} \rangle$ taken at $\mathbf{q} = \mathbf{b}_1 + \mathbf{b}_2$, $\mathbf{q} = 2\mathbf{b}_1$, respectively. The DTH ansatz, on the contrary, describes somewhat DTHs even at fields $b \simeq b_{cr2}$, with insignificant admixture of higher harmonics. As a result, we see in Fig. 5 that the values of $C_{11}/C_{10}$ and $C_{20}/C_{10}$ predicted by the SkX approach are much larger than for DTH near the melting transition, $b \simeq b_{cr2}$.

According to Refs. [23,24] (see also Ref. [29]), the perfect SkX is melted before undergoing a uniform FM state at $b > b_{cr2}$. Our predictions for the ratio of amplitudes $C_{ij}/C_{10}$ should partly survive in the intermediate skyrmion liquid phase. Instead of well-defined Bragg peaks, one observes concentric circles, corresponding to short-range order in the isotropic state. The above intensities $C_{10}$, $C_{11}$, $C_{20}$ should then be associated with the integrated intensities near $|q| = k$, $|q| = k\sqrt{3}$, $|q| = 2k$, respectively.

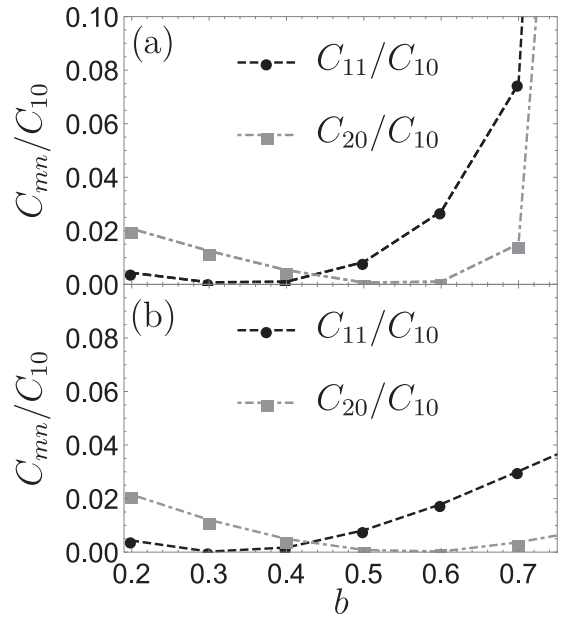


FIG. 5. Relative intensities $C_{11}/C_{10}$ and $C_{20}/C_{10}$ for various external magnetic fields, calculated with (a) skyrmion crystal Eq. (7) approach and (b) deformed triple helix Eq. (18), respectively.

At the same time, the above predictions for $C_{11}$, $C_{20}$ cannot be simply compared to Lorentz TEM results [23,24], where the profile of skyrmions has been modeled by $\delta$ function, $\delta(r - r_j)$, as opposed to the above Eqs. (3) and (4).

## VI. CONCLUSIONS

We considered several variants to describe the SkX, formed at $T = 0$ in a 2D model of a ferromagnet with DMI and the magnetic field. The first variant is the modification of the stereographic projection method used in the seminal paper [26] for the pure $O(3)$ sigma model. The second approach is the generalization of the triple helix ansatz Eq. (18). The third variant is the combination of the stereographic projection with the triple helix description.

The numerical analysis of the classical energy shows that the first two approaches yield very close estimates at intermediate values of an external magnetic field, $b$, but are different at lower and higher magnetic fields, close to critical fields characterizing the transitions either to single helix or to uniform FM phase. The third approach leads to the higher energy than the first two approaches in the whole region of $b$.

Comparing to other methods, the stereographic projection ansatz appears more appropriate at higher magnetic fields, providing lower energy estimates and predicting a growing distance between skyrmions. It is yet to be checked whether this conclusion is affected by including into our model other types of magnetic interaction, e.g., uniaxial anisotropy or magnetostatic (dipolar) interaction.

In contrast to the skyrmion A phase in bulk materials observed at high temperatures, $\sim T_C$, the SkXoccurring at low temperatures for the 2D case or in layered compounds should lead to sizable secondary Bragg peaks. The intensity of these peaks is nonzero for the saturated local magnetization and depends on details of magnetic structure at low temperatures. Our modeling shows that the intensities of secondary Bragg peaks $C_{11}$ and $C_{20}$ are of the order of a few percent of the primary intensity, $C_{10}$. These estimates result from the form factor of individual skyrmions and should apparently survive the melting transition to the skyrmion liquid phase at higher fields.

In conclusion, analyzing the topologically nontrivial ground state of the standard model of chiral 2D magnets, we show that its description near the transition to the FM uniform state is preferable within the stereographic projection method. An investigation of the secondary Bragg reflexes in the skyrmion state can give additional information about the magnetic profile of individual skyrmions.

## ACKNOWLEDGMENTS

We thank E.V. Altynbaev and S.V. Grigoriev for useful discussions. The work of V.T. was supported by the Foundation for the Advancement of Theoretical Physics BASIS. The work of D.A. was funded in part by the Russian Foundation for Basic Research (Grant No. 20-52-12019)–Deutsche Forschungsgemeinschaft (Grant No. SCHM 1031/12-1) cooperation.

[1] T. Skyrme, Nucl. Phys. **31**, 556 (1962).
[2] N. Nagaosa and Y. Tokura, Nat. Nanotechnol. **8**, 899 (2013).
[3] M. Garst, J. Waizner, and D. Grundler, J. Phys. D **50**, 293002 (2017).
[4] W. Koshibae, Y. Kaneko, J. Iwasaki, M. Kawasaki, Y. Tokura, and N. Nagaosa, Jpn. J. Appl. Phys. **54**, 053001 (2015).
[5] R. Tomasello, E. Martinez, R. Zivieri, L. Torres, M. Carpentieri, and G. Finocchio, Sci. Rep. **4**, 6784 (2014).
[6] G. Derrick, J. Math. Phys. **5**, 1252 (1964).
[7] K. L. Metlov, Phys. Rev. B **88**, 014427 (2013).
[8] A. Fert, V. Cros, and J. Sampaio, Nat. Nanotechnol. **8**, 152 (2013).
[9] I. Dzyaloshinskii, Sov. Phys. JETP **19**, 960 (1964).
[10] A. N. Bogdanov and D. Yablonskii, Zh. Eksp. Teor. Fiz **95**, 178 (1989).
[11] S. Mühlbauer, B. Binz, F. Jonietz, C. Pfleiderer, A. Rosch, A. Neubauer, R. Georgii, and P. Böni, Science **323**, 915 (2009).
[12] T. Adams, S. Mühlbauer, C. Pfleiderer, F. Jonietz, A. Bauer, A. Neubauer, R. Georgii, P. Böni, U. Keiderling, K. Everschor, M. Garst, and A. Rosch, Phys. Rev. Lett. **107**, 217206 (2011).
[13] X. Yu, Y. Onose, N. Kanazawa, J. Park, J. Han, Y. Matsui, N. Nagaosa, and Y. Tokura, Nature **465**, 901 (2010).
[14] T. H. R. Skyrme, Proc. Roy. Soc. London A **262**, 237 (1961).
[15] J. Perring and T. Skyrme, Nucl. Phys. **31**, 550 (1962).
[16] I. Dzyaloshinskii, Sov. Phys. JETP **20**, 665 (1965).
[17] A. Borisov and V. Kiseliev, Physica D **31**, 49 (1988).
[18] D. N. Aristov and A. Luther, Phys. Rev. B **65**, 165412 (2002).
[19] A. B. Borisov, J.-i. Kishine, I. G. Bostrem, and A. S. Ovchinnikov, Phys. Rev. B **79**, 134436 (2009).
[20] G. Tatara and H. Fukuyama, J. Phys. Soc. Jpn. **83**, 104711 (2014).
[21] T. Kaplan, Phys. Rev. **124**, 329 (1961).
[22] V. Timofeev, A. Sorokin, and D. Aristov, JETP Lett. **109**, 207 (2019).
[23] R. Seshadri and R. M. Westervelt, Phys. Rev. Lett. **66**, 2774 (1991).
[24] P. Huang, T. Schönenberger, M. Cantoni, L. Heinen, A. Magrez, A. Rosch, F. Carbone, and H. M. Rønnow, Nat. Nanotechnol. **15**, 761 (2020).
[25] Y. A. Izyumov, Soviet Physics Uspekhi **27**, 845 (1984).
[26] A. A. Belavin and A. M. Polyakov, JETP Lett. **22**, 245 (1975).
[27] A. Bogdanov and A. Hubert, J. Magn. Magn. Mater. **138**, 255 (1994).
[28] G. L. Squires, *Introduction to the Theory of Thermal Neutron Scattering* (Cambridge University Press, Cambridge, 2012).
[29] S. V. Grigoriev, N. Potapova, E. Moskvin, V. Dyadkin, C. Dewhurst, and S. V. Maleyev, JETP Lett. **100**, 216 (2014).